Investigation of Hydrogen Incorporations in Bulk Infinite-Layer Nickelates

P. Puphal[1]*, V. Pomjakushin[2], R. A. Ortiz[1], S. Hammoud[3], M. Isobe[1], B. Keimer[1] and M. Hepting[1]

[1]Max-Planck-Institute for Solid State Research, Stuttgart, Germany, [2]Laboratory for Neutron Scattering and Imaging (LNS), Paul Scherrer Institute (PSI), Villigen, Switzerland, [3]Max-Planck-Institute for Intelligent Systems, Stuttgart, Germany

Infinite-layer (IL) nickelates are an emerging class of superconductors, where the Ni^{1+} valence state in a square planar NiO_2 coordination can only be reached *via* topotactic reduction of the perovskite phase. However, this topotactic soft chemistry with hydrogenous reagents is still at a stage of rapid development, and there are a number of open issues, especially considering the possibility of hydrogen incorporation. Here, we study the time dependence of the topotactic transformation of $LaNiO_3$ to $LaNiO_2$ for powder samples with x-ray diffraction and gas extraction techniques. While the hydrogen content of the powder increases with time, neutron diffraction shows no negative scattering of hydrogen in the $LaNiO_2$ crystal lattice. The extra hydrogen appears to be confined to grain boundaries or secondary-phase precipitates. The average crystal structure, and possibly also the physical properties, of the primary $LaNiO_2$ phase are, therefore, not noticeably affected by hydrogen residues created by the topotactic transformation.

Keywords: infinite-layer nickelates, topotactic reduction, superconductivity, neutron diffraction, gas extraction, x-ray diffraction, hydrogen

1 INTRODUCTION

Superconductivity exists in various hydrogen-containing compounds, highlighted by the recent discoveries of critical temperatures T_c as high as room temperature for hydride compounds formed under extreme pressures [1, 2]. Metal hydroxide–intercalated iron chalcogenides, such as $(Li_{0.8}Fe_{0.2})OHFeSe$ [3], show coexistence of antiferromagnetic order and superconductivity, a feature known from some high-T_c superconductors [4]. Electron-doped 1111 iron pnictides, such as $RFeAsO_{1−x}H_x$ [5, 6], $CeFeAsO_{1−x}H_x$ [7], and the pnictogen-free LaFeSiH [8] are a class, where the introduction of charge carriers *via* doping with hydrogen drives the system from an antiferromagnetically ordered state toward superconductivity. In layered sodium cobalt oxyhydrate, $Na_xCoO_2·H_2O$ [9], superconductivity with a similar hole/electron-doping behavior by chemical substitution is observed as in the cuprate high-T_c superconductors [10].

For IL nickelates, a close relation and possible analogy to cuprate superconductors was suggested already in 1999 [11], and since the first discovery of superconductivity in the IL nickelate $(Nd,Sr)NiO_2$ [12], the observation of superconductivity has been confirmed [13–15] and extended to $(Pr,Sr)NiO_2$ [16], $(La,Sr)NiO_2$ [17], $(La,Ca)NiO_2$ [18], and $Nd_6Ni_5O_{12}$ [19]. Furthermore, a recent work reported superconductivity not only for films grown on $SrTiO_3$ substrates but also on LSAT [20], which provides enough evidence to consider thin-film nickelates as a novel class of superconductors. The possible

presence of topotactic hydrogen in IL nickelates, which depends on the rare-earth ion and/or epitaxial strain [21, 22], was proposed in theoretical studies [23, 24] and might have substantial influence on the electronic and magnetic properties of the IL nickelates, as $LaNiO_2H$ would realize a two-orbital Mott insulator [23]. A hint toward the possibility of hydrogen incorporation was provided by an early study of topotactically reduced $NdNiO_3$ films, which showed an oxyhydride $NdNiO_{3-x}H_y$ phase with a defect-fluorite structure in the surface region [25]. Furthermore, topotactic hydrogen can be found in $SrTiO_3$ thin films [26], that is, the material that is commonly used as a substrate and capping layer for IL nickelate films, which again provides a possible route for inclusion of hydrogen in infinite-layer nickelate thin films. While superconductivity has remained elusive in IL nickelates in bulk form, with studies on powder samples reporting insulating behavior [27, 28], a first step toward superconductivity was taken by our recent investigation of $(La,Ca)NiO_2$ single crystals [29], where metallicity was observed.

In this study, we address the issue of possible hydrogen incorporations in IL nickelates by examining bulk $LaNiO_{3-x}H_y$ powder samples with a combination of x-ray and neutron diffraction studies, gas extraction, and complementary high-pressure synthesis attempts of $LaNiO_2H$.

2 METHODS

$LaNiO_3$ powder samples with grain sizes of $0.5\,\mu m$ were synthesized *via* the citrate–nitrate method as described in Ref. [30]. The method is optimal as the relatively small grains enhance the surface to bulk ratio, reducing reduction times. Moreover, higher purity can be reached than by high-pressure powder synthesis. The IL phase $LaNiO_2$ can be obtained solely through topotactic reduction of the perovskite $LaNiO_3$ phase, which is here achieved by using CaH_2 as the reducing agent [27, 28]. We reduced 50 mg of $LaNiO_3$ powder wrapped in aluminum foil, spatially separated from 250 mg CaH_2 powder at 280°C, as described in detail in Ref. [30], for various times.

We measured the stoichiometry including the hydrogen content with a combination of inductively coupled plasma mass spectroscopy (ICP-OES) and gas extraction; the former with a SPECTRO CIROS CCD and the latter with an Eltra ONH-2000 analyzer. For the determination of oxygen and hydrogen content, the powder samples were placed in a Ni crucible and clipped and heated, where the carrier gas takes the oxygen and hydrogen out of the sample. The oxygen reacts with carbon, and CO_2 is detected in an infrared cell, while hydrogen is detected by a thermal conductivity cell. Each measurement is repeated three times and compared to a standard. The quoted error bars provide the statistical error.

Powder x-ray diffraction (PXRD) data were collected using a Rigaku MiniFlex with a Cu K_α tube at room temperature. Neutron diffraction was performed at the high-resolution powder neutron diffractometer HRPT [31] at the Spallation Neutron Source SINQ at the Paul Scherrer Institute in Villigen. For the HRPT experiments, an amount of 340 mg of
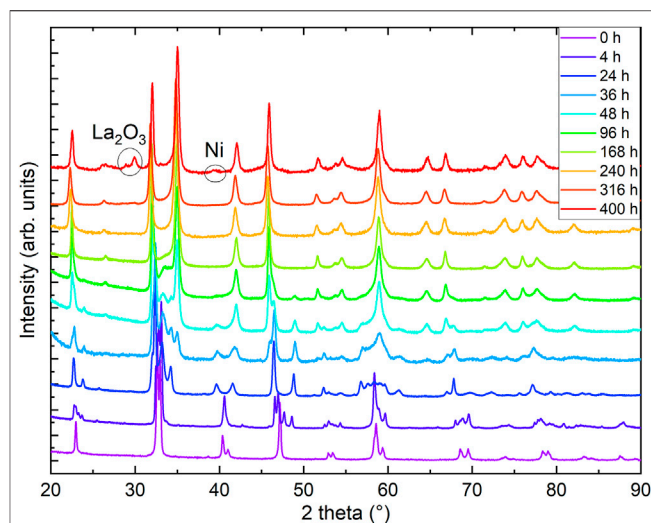

FIGURE 1 | Powder x-ray diffraction (PXRD) of reduced $LaNiO_3$ after different reduction times. Data were measured at T = 300 K with Cu K_α radiation. Curves are offset in vertical direction for clarity. The 0- and 316-h data are reproduced from Ref. [30].

$LaNiO_2$ was enclosed into a vanadium can with an inner diameter of 6 mm, where the remaining space of the vanadium can was shielded with Cd foil, and the measurement was carried out at 1.5 K in a ^{4}He bath cryostat with a neutron wavelength of 1.15 Å.
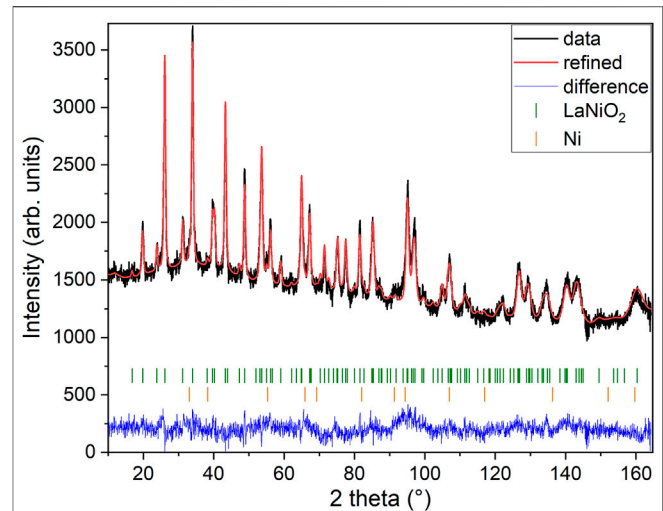
3 RESULTS

As a first step, we checked the purity and stoichiometry of our starting material in the perovskite phase. In PXRD, we found no detectable impurities, and ICP combined with measurements of gas extraction indicated a starting stoichiometry of $La_{0.99(1)}$ $Ni_{0.99(1)}O_{2.99(3)}H_{0.005(2)}$. We studied the reduction progress with time in detail by preparation of several ampules and extracting samples after varying reduction times and analyzed all the products with PXRD. We noticed that the progress of the reduction depends on the purity and sample amount and grain size for a given time as the reduction process is surface-dependent. Motivated by these observations, we carried out a standardized reduction on the same batch of perovskite precursors. After 1 day of reduction in the described process (see **Section 2**) we found a full structural transition to $LaNiO_{2.5}$ (see **Figure 1**). Our Rietveld refinement of the $LaNiO_{2.5}$ crystal structure is in good agreement with previous reports on reduced powder [32–34]. Notably, reduction times of 1 day and longer are in stark contrast to thin-film samples, which can be fully reduced to the IL phase within hours [12–18, 35, 36], presumably due to the enhanced thickness of our grains, with sizes of $0.5\,\mu m$ as extracted from scanning electron microscopy (SEM) images. The reduction appears to be happening in domains, as we found cluster spin glass behavior in a detailed magnetic characterization [30], and thus after longer reduction times than 1 day, we observe phase mixtures of $LaNiO_{2.5}$ in $P2_1/n$ (#14) [33] and $LaNiO_2$ in $P4/mmm$ (#123) [37], with a slowly increasing fraction of the $LaNiO_2$
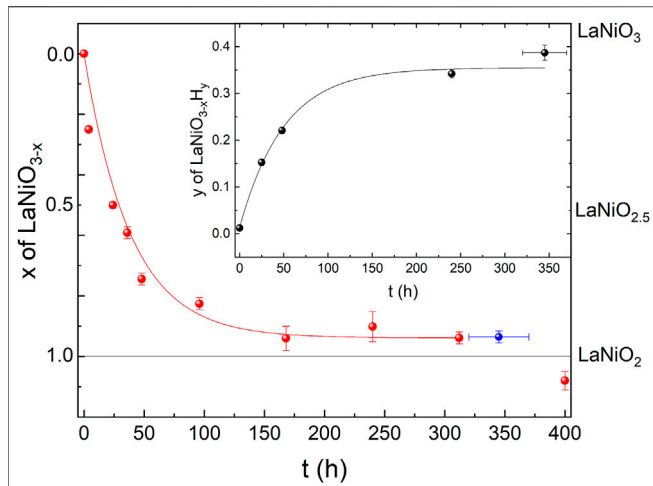
FIGURE 2 | Oxygen and hydrogen content of reduced $LaNiO_3$ after different reduction times. Red symbols correspond to the oxygen content x in $LaNiO_{3-x}$, extracted from Rietveld refinements of the PXRD data shown in **Figure 1**. The blue datapoint is extracted from Rietveld refinement of our neutron diffraction data shown in **Figure 3**. The solid red line is a guide to the eye. The black symbols in the inset correspond to the hydrogen content y in $LaNiO_{3-x}H_y$, obtained from gas extraction. The solid black line is a guide to the eye.

FIGURE 3 | Neutron powder diffraction. The data are taken from mixed samples reduced in the range of 320–376 h. The Rietveld refinement includes the $LaNiO_2$ phase and a Ni minority phase. Data were collected at 1.5 K with a neutron wavelength of 1.15 Å.

phase as a function of time (see **Figure 2**). Extracting the weight percentages from our refinement, we present the reduction progress for the CaH_2 reduction in analogy to a thermogravimetry (TG) curve, which is shown in **Figure 2**. The reduction process follows an exponential decay, which we also observed in thermogravimetry studies in hydrogen gas flow (not shown here). After a reduction time of approximately 316 h, the crystal structure can be refined assuming a single phase of IL $LaNiO_2$ (**Figure 2**, and Ref. [30]). Notably, while the structural transition does not progress further on an exponential time scale, a small amount of apical oxygen remains in the crystal lattice, as will be revealed by neutron diffraction below. However, for even longer reduction times, the sample begins to decompose, forming Ni and La_2O_3, which becomes clearly visible in PXRD after 400 h (**Figures 1**, **2**).

In the inset of **Figure 2**, we plot the hydrogen content in the resulting powder samples versus reduction time, obtained by a gas extraction method. While the initial perovskite nickelate shows a hydrogen content of 0.005(2) wt%, we find increase of hydrogen with time (opposite to the oxygen content), with 0.065(3) wt% for 24 h, 0.094(3) wt% for 38 h, 0.015(5) wt% for 240 h, and finally 0.169(7) wt% after 320–376 h. *Via* gas extraction, we find an oxygen content of 14.1(2) wt% after 316 h and 14.0(2) wt% after 320–376 h of reduction, where 14 wt% corresponds to a full reduction to the $LaNiO_2$ IL phase. If we assume that the amount of hydrogen would be incorporated into the average crystal structure, the corresponding effective stoichiometry of the sample investigated with neutrons would be $La_{0.99(1)}Ni_{0.99(1)}O_{2.00(2)}H_{0.39(2)}$, where La and Ni are determined *via* ICP. However, a first hint that this might not be the case comes from the presence of small amounts of elemental

TABLE 1 | Refined atomic coordinates of $LaNiO_2$ in tetragonal space group $P4/mmm$ with preferred orientation extracted from powder neutron diffraction data at 1.5 K (**Figure 3**).

$LaNiO_2$	$a, b = 3.9550(3)$ Å, $c = 3.3588(3)$ Å				
Atom	x	y	z	$U[Å^2]$	**Occ**
La (1d)	0.5	0.5	0.5	0.0036(6)	1
Ni (1a)	0	0	0	0.0057(5)	1
O (2f)	0	0.5	0	0.0098(5)	1
O (1b)	0	0	0.5	0.0098(5)	0.06(1)
Reliability factors	χ^2	R_B	R_f		
	1.89	3.53	2.79		

Ni in the PXRD of the 400-h sample (**Figure 1**), which is known to trap hydrogen [38]. The Rietveld refinement of the neutron diffraction data below also indicates a small amount of Ni. Furthermore, signatures of Ni precipitates (below the detection threshold of our PXRD) were also detected in powders after shorter reduction times since they give rise to ferromagnetic contributions in the magnetic signal [30]. The amount of Ni likely increases with reduction time, which could explain the increasing capability of incorporating hydrogen.

As a next step, we performed high-resolution neutron diffraction experiments on 340 mg of a sample prepared by mixing batches that had been subject to reduction times of 320, 350, and 376 h, respectively which are all in the range just before the start of the clear decay shown in **Figure 2**. The obtained neutron diffraction pattern can be well refined (see **Figure 3**) assuming $LaNiO_2$ in the IL $P4/mmm$ structure (see **Table 1**), with a c-axis parameter of 3.3588(3) Å, which is lower than previously reported values [29, 30, 37], and 1.1(2) wt% of elemental Ni was included as a secondary phase.
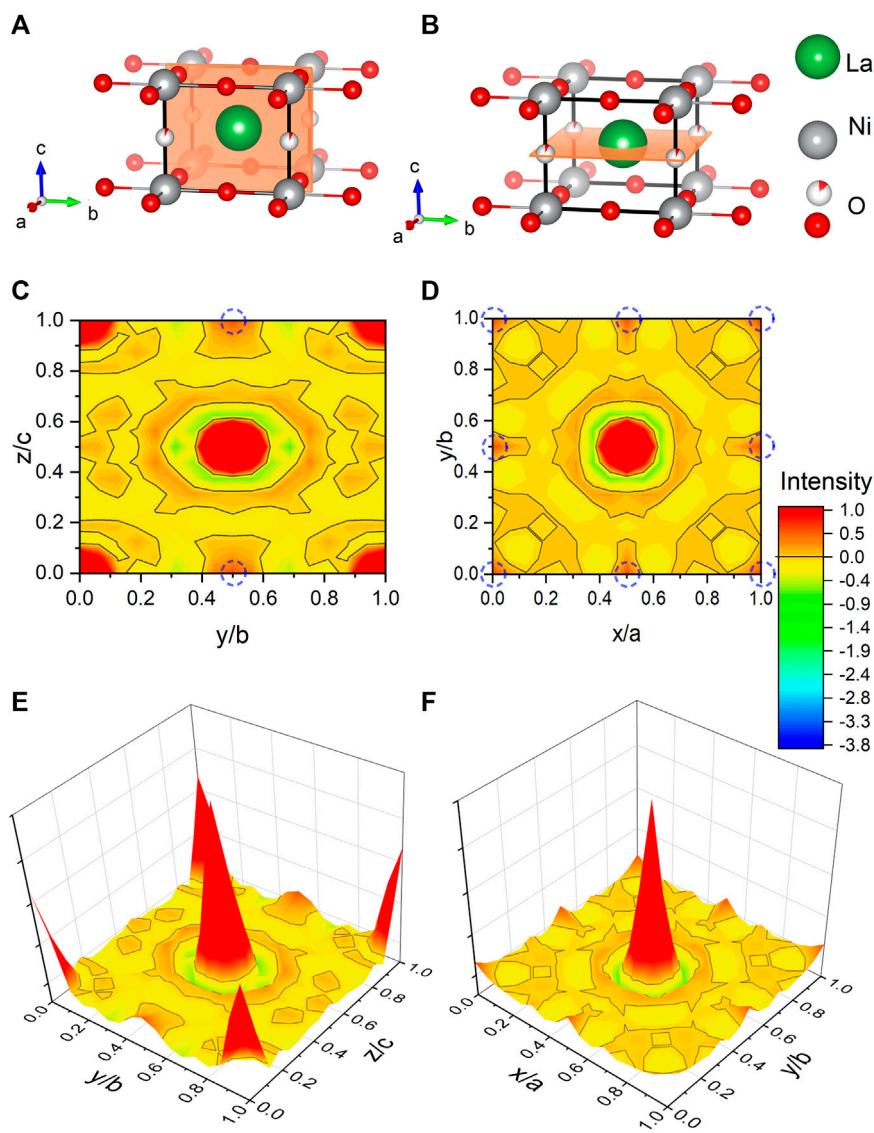
FIGURE 4 | Fourier maps of the scattering length density within the unit cell of LaNiO$_2$ extracted from neutron powder diffraction. **(A,B)** Refined unit cells with cuts corresponding to the Fourier maps in **(C,D)**, with the intensity range focused on the negative scattering length (yellow to blue), with −3.74 fm corresponding to hydrogen [40]. The positive scattering (orange to red) is capped at 1 (with 5.8 fm corresponding to oxygen). The black lines mark the isosurface lines with zero scattering intensity. The theoretically proposed hydrogen positions [23, 24] are highlighted with blue dashed circles. **(E,F)** Fourier maps are shown as a 3D colormap.

Figure 4 shows a Fourier map of the scattering density resulting from the Rietveld refinement of the neutron data, where the range of the color scheme is chosen to focus on the negative scattering length of hydrogen. While the used reduction temperatures (see **Section 2**) are too low to enable significant mobility of the La and Ni ions, the purpose of our topotactic treatment is to reduce oxygen, which becomes mobile and is extracted by reaction with hydrogen. We, therefore, focus on the scattering lengths of the two elements O and H. According to the theoretical prediction of Ref. [23], intercalation of H in IL nickelates is most favorable on the vacant apical oxygen sites with Wyckoff position (1b), or on interstitial positions between the rare-earth ions (Wyckoff positions (2e) and (1c)). Another

theoretical work [24] predicts that NdNiO$_2$ is unstable, while NdNiO$_2$H is not and also proposes the apical oxygen site with Wyckoff position (1b) for hydrogen. However, as shown in the Fourier maps of **Figure 4**, we find no significant negative scattering, which would appear as blue in our plots. The slightly negative scattering realized as a ring around a reflex, here in close proximity to La, is an artifact from the Fourier transformation, typically seen around larger ions [39] due to a signal cutoff from a finite q range. This is best seen in the Fourier maps **Figures 4E,F**. We note that the data can be refined with similar reliability factors as in **Table 1** by putting a mixture of O and H on Wyckoff position (1b) and constraining their occupation. As the positive scattering observed at this site

could be a mixture of negative scattering of H and positive scattering of O, which effectively clouds the negative scattering. Realized in a substitution series with $LaNiO_{3-x}H_x$, which would yield occupations of O: 0.430(8) and H: 0.570(8) in refinements of our data, but this oxygen content is way higher than what can be found in multiple gas extraction experiments $(La_{0.99(1)}Ni_{0.99(1)}O_{2.00(2)}H_{0.39(2)})$. Most importantly, the scenario of $LaNiO_{3-x}H_x$ would hint toward the possibility to synthesize the phase directly, similar as observed in the iron pnictides. However, such synthesis attempts have been carried out as described below and were not successful. Furthermore, in the case of iron pnictides, hydrogen substitution leads to no structural transitions [5–7], contrasting the evolution of the underlying structural transitions in $LaNiO_{3-x}$ according to the PXRD data (see **Figure 1**) and literature [37]. Another possibility to refine mixed occupancy is by constraining an equal occupation of O and H as $LaNiO_2(OH)_x$, which converges to 0.18(4). However, this would rather suggest an OH molecule with typical distances around 0.84 Å, which would realize negative scattering [39] and, thus, reduces the quality of the fit and shifts the occupation again down to 0.06(1). Thus, we conclude that intercalated hydrogen is unlikely in our $LaNiO_{2+\delta}$ powder sample. Nevertheless, we find the presence of a small amount of residual apical oxygen in Wyckoff position (1b), which corresponds to a deviation of $\delta = 0.06(1)$ from the ideal stoichiometry.

In addition, we attempted direct synthesis approaches of $LaNiO_{3-x}H_x$ as, for example, $LaNiO_2H$ *via* a Walker-type high-pressure synthesis in NaCl crucibles. We mixed La_2O_3 and NiO with NaH or CaH_2 and heated it to 650–1000°C under a pressure of 5–7 GPa, but were unable to synthesize any oxyhydride nickelate. Instead, we obtained $La(OH)_3$ and Ni, which is in contrast to related cases, such as $SmFeAsO_{1-x}H_x$ [5], $BaCrO_2H$ [41], $BaScO_2H$ [42], and $SrVO_2H$ [43].

4 CONCLUSION

In summary, we have synthesized high-quality $LaNiO_{2+\delta}$ powders and found some density of residual oxygen ($\delta = 0.06(1)$) even at the final stage of the topotactic reaction, just prior to decomposition of our samples. While our gas extraction method reveals partial hydrogen inclusions in the powder samples, high-resolution neutron diffraction refinements show that there is no clear topotactic hydrogen in $LaNiO_2$, and direct attempts to synthesize $LaNiO_{3-x}H_x$ were unsuccessful. The

hydrogen detected by gas extraction could be trapped in Ni impurities that increase with increasing reduction time and/or ascribed to phenomena at surfaces or grain boundaries, such as water adsorption/intercalation [44] on powder surfaces or partial formation of $LaNiO_{3-x}H_x$ on the nanometer scale [25]. Notably, a relatively high density of grain boundaries/crystallographic defects was reported for IL nickelate thin films [45], and also surface effects can play a more decisive role in films. Thus, future studies clarifying the presence and impact of hydrogen in nickelate thin-film samples are highly desirable.

DATA AVAILABILITY STATEMENT

The raw data supporting the conclusion of this article will be made available by the authors, without undue reservation.

AUTHOR CONTRIBUTIONS

PP, MI, BK, and MH conceived the project. RO carried out the topotactic reductions. PP and VP conducted the neutron diffraction experiments. SH executed the ICP and gas extraction measurements. PP analyzed the data and prepared the manuscript with input from all authors.

FUNDING

ACKNOWLEDGMENTS

REFERENCES

1. Shamp A, Zurek E Superconductivity in Hydrides Doped with Main Group Elements Under Pressure. *Nov Supercond Mater* (2017) 3:14. doi:10.1515/nsm-2017-0003

2. Snider E, Dasenbrock-Gammon N, McBride R, Debessai M, Vindana H, Vencatasamy K, et al. Room-temperature Superconductivity in a Carbonaceous Sulfur Hydride. *Nature* (2020) 586:373–7. doi:10.1038/s41586-020-2801-z

3. Lu XF, Wang NZ, Wu H, Wu YP, Zhao D, Zeng XZ, et al. Coexistence of Superconductivity and Antiferromagnetism in (Li0.8Fe0.2)OHFeSe. *Nat Mater* (2014) 14:325–9. doi:10.1038/nmat4155

4. Kahsay G, Singh P. Coexistence of Superconductivity and Antiferromagnetism in High-T C Gd1+x Ba2−x Cu3O7−δ Superconductor. *J Supercond Nov Magn* (2016) 29:2031–4. doi:10.1007/s10948-016-3549-4

5. Hanna T, Muraba Y, Matsuishi S, Igawa N, Kodama K, Shamoto S-i., et al. Hydrogen in layered iron arsenides: Indirect electron doping to induce superconductivity. *Phys Rev B* (2011) 84:024521. doi:10.1103/physrevb.84.024521

6. Hiraishi M, Iimura S, Kojima KM, Yamaura J, Hiraka H, Ikeda K, et al. Bipartite Magnetic Parent Phases in the Iron Oxypnictide Superconductor. *Nat Phys* (2014) 10:300–3. doi:10.1038/nphys2906

7. Matsuishi S, Hanna T, Muraba Y, Kim SW, Kim JE, Takata M, et al. Structural analysis and superconductivity of CeFeAsO$_{1-x}$H$_x$. *Phys Rev B* (2012) 85:014514. doi:10.1103/physrevb.85.014514

8. Bernardini F, Garbarino G, Sulpice A, Núñez-Regueiro M, Gaudin E, Chevalier B, et al. Iron-based Superconductivity Extended to the Novel Silicide LaFeSiH. *Phys Rev B* (2018) 97. doi:10.1103/physrevb.97.100504

9. Lynn JW, Huang Q, Brown CM, Miller VL, Foo ML, Schaak RE, et al. Structure and Dynamics of superconductingNaxCoO2hydrate and its Unhydrated Analog. *Phys Rev B* (2003) 68:214516. doi:10.1103/physrevb.68.214516

10. Keimer B, Kivelson SA, Norman MR, Uchida S, Zaanen J. From Quantum Matter to High-Temperature Superconductivity in Copper Oxides. *Nature* (2015) 518:179–86. doi:10.1038/nature14165

11. Anisimov VI, Bukhvalov D, Rice TM. Electronic Structure of Possible Nickelate Analogs to the Cuprates. *Phys Rev B* (1999) 59:7901–6. doi:10.1103/physrevb.59.7901

12. Li D, Lee K, Wang BY, Osada M, Crossley S, Lee HR, et al. Superconductivity in an Infinite-Layer Nickelate. *Nature* (2019) 572:624–7. doi:10.1038/s41586-019-1496-5

13. Zeng S, Tang CS, Yin X, Li C, Li M, Huang Z, et al. Phase Diagram and Superconducting Dome of Infinite-Layer Nd1−xSrxNiO2 Thin Films. *Phys Rev Lett* (2020) 125:147003. doi:10.1103/physrevlett.125.147003

14. Li Y, Sun W, Yang J, Cai X, Guo W, Gu Z, et al. Impact of Cation Stoichiometry on the Crystalline Structure and Superconductivity in Nickelates. *Front Phys* (2021) 9:443. doi:10.3389/fphy.2021.719534

15. Gao Q, Zhao Y, Zhou X-J, Zhu Z. Preparation of Superconducting Thin Films of Infinite-Layer Nickelate Nd0.8Sr0.2NiO2. *Chin Phys. Lett.* (2021) 38:077401. doi:10.1088/0256-307x/38/7/077401

16. Osada M, Wang BY, Goodge BH, Lee K, Yoon H, Sakuma K, et al. A Superconducting Praseodymium Nickelate with Infinite Layer Structure. *Nano Lett* (2020) 20:5735–40. doi:10.1021/acs.nanolett.0c01392

17. Osada M, Wang BY, Goodge BH, Harvey SP, Lee K, Li D, et al. Nickelate Superconductivity without Rare-Earth Magnetism: (La,Sr)NiO 2. *Adv Mater* (2021) 33:2104083. doi:10.1002/adma.202104083

18. Zeng SW, Li CJ, Chow LE, Cao Y, Zhang ZT, Tang CS, et al. *Superconductivity in Infinite-Layer Lanthanide Nickelates* (2021). arXiv:2105.13492 [cond-mat.supr-con].

19. Pan GA, Ferenc Segedin D, LaBollita H, Song Q, Nica EM, Goodge BH, et al. Superconductivity in a Quintuple-Layer Square-Planar Nickelate. *Nat Mater* (2021) 21:160–4. doi:10.1038/s41563-021-01142-9

20. Ren X, Gao Q, Zhao Y, Luo H, Zhou X, Zhu Z. *Superconductivity in Infinite-Layer pr0.8sr0.2nio2 Films on Different Substrates* (2021). arXiv:2109.05761 [cond-mat.supr-con].

21. Bernardini F, Bosin A, Cano A. *Geometric Effects in the Infinite-Layer Nickelates* (2021). arXiv:2110.13580 [cond-mat.supr-con].

22. Alvarez AAC, Petit S, Iglesias L, Prellier W, Bibes M, Varignon J. *Structural Instabilities of Infinite-Layer Nickelates from First-Principles Simulations* (2021). arXiv:2112.02642 [cond-mat.mtrl-sci].

23. Si L, Xiao W, Kaufmann J, Tomczak JM, Lu Y, Zhong Z, et al. Topotactic Hydrogen in Nickelate Superconductors and Akin Infinite-Layer Oxides ABO2. *Phys Rev Lett* (2020) 124:166402. doi:10.1103/physrevlett.124.166402

24. Malyi OI, Varignon J, Zunger A. *Bulk Ndnio2 Is Thermodynamically Unstable with Respect to Decomposition while Hydrogenation Reduces the Instability and Transforms it from Metal to Insulator* (2021). doi:10.1103/PhysRevB.105.014106

25. Onozuka T, Chikamatsu A, Katayama T, Fukumura T, Hasegawa T. Formation of Defect-Fluorite Structured NdNiOxHy Epitaxial Thin Films via a Soft Chemical Route from NdNiO3 Precursors. *Dalton Trans* (2016) 45:12114–8. doi:10.1039/c6dt01737a

26. Kutsuzawa D, Hirose Y, Chikamatsu A, Nakao S, Watahiki Y, Harayama I, et al. Strain-enhanced Topotactic Hydrogen Substitution for Oxygen in SrTiO3epitaxial Thin Film. *Appl Phys Lett* (2018) 113:253104. doi:10.1063/1.5057370

27. Wang B-X, Zheng H, Krivyakina E, Chmaissem O, Lopes PP, Lynn JW, et al. Synthesis and characterization of bulk Nd1−x SrxNi O 2 and Nd1−x Srx NiO3. *Phys Rev Mater* (2020) 4:084409. doi:10.1103/physrevmaterials.4.084409

28. Li Q, He C, Si J, Zhu X, Zhang Y, Wen H-H. Absence of Superconductivity in Bulk Nd1−xSrxNiO2. *Commun Mater* (2020) 1:16. doi:10.1038/s43246-020-0018-1

29. Puphal P, Wu Y-M, Fürsich K, Lee H, Pakdaman M, Bruin JAN, et al. Topotactic transformation of single crystals: From perovskite to infinite-layer nickelates. *Sci Adv* (2021) 7:eabl8091. doi:10.1126/sciadv.abl8091

30. Ortiz RA, Puphal P, Klett M, Hotz F, Kremer RK, Trepka H, et al. *Magnetic Correlations in Infinite-Layer Nickelates: An Experimental and Theoretical Multi-Method Study* (2021). arXiv:2111.13668 [cond-mat.str-el].

31. Fischer P, Frey G, Koch M, Könnecke M, Pomjakushin V, Schefer J, et al. High-resolution Powder Diffractometer HRPT for thermal Neutrons at SINQ. *Physica B: Condensed Matter* (2000) 276-278:146–7. doi:10.1016/s0921-4526(99)01399-x

32. Crespin M, Levitz P, Gatineau L. Reduced Forms of LaNiO3perovskite. Part 1.-Evidence for New Phases: La2Ni2O5and LaNiO2. *J Chem Soc Faraday Trans 2* (1983) 79:1181–94. doi:10.1039/f29837901181

33. Alonso JA, Martínez-Lope MJ. Preparation and crystal Structure of the Deficient Perovskite LaNiO2.5, Solved from Neutron Powder Diffraction Data. *J Chem Soc Dalton Trans* (1995) 2819–24. doi:10.1039/dt9950002819

34. Alonso JA, Martínez-Lope MJ, García-Muñoz JL, Fernández-Díaz MT. A Structural and Magnetic Study of the Defect Perovskite LaNiO2.5 from High-Resolution Neutron Diffraction Data. *J Phys Condensed Matter* (1997) 9:6417–6426.

35. Ikeda A, Krockenberger Y, Irie H, Naito M, Yamamoto H. Direct Observation of Infinite NiO2planes in LaNiO2films. *Appl Phys Express* (2016) 9:061101. doi:10.7567/apex.9.061101

36. Hepting M, Li D, Jia CJ, Lu H, Paris E, Tseng Y, et al. Electronic Structure of the Parent Compound of Superconducting Infinite-Layer Nickelates. *Nat Mater* (2020) 19:381–5. doi:10.1038/s41563-019-0585-z

37. Hayward MA, Green MA, Rosseinsky MJ, Sloan J. Sodium Hydride as a Powerful Reducing Agent for Topotactic Oxide Deintercalation: Synthesis and Characterization of the Nickel(I) Oxide LaNiO2. *J Am Chem Soc* (1999) 121:8843–54. doi:10.1021/ja991573i

38. Louthan MR, Donovan JA, Caskey GR. Hydrogen Diffusion and Trapping in Nickel. *Acta Metallurgica* (1975) 23:745–9. doi:10.1016/0001-6160(75)90057-7

39. Sano-Furukawa A, Hattori T, Komatsu K, Kagi H, Nagai T, Molaison JJ, et al. Direct Observation of Symmetrization of Hydrogen Bond in δ-AlOOH under Mantle Conditions Using Neutron Diffraction. *Sci Rep* (2018) 8. doi:10.1038/s41598-018-33598-2

40. Sears VF. Neutron Scattering Lengths and Cross Sections. *Neutron News* (1992) 3:26–37. doi:10.1080/10448639208218770

41. Higashi K, Ochi M, Nambu Y, Yamamoto T, Murakami T, Yamashina N, et al. Enhanced Magnetic Interaction by Face-Shared Hydride Anions in 6H-BaCrO2H. *Inorg Chem* (2021) 60:11957–63. doi:10.1021/acs.inorgchem.1c00992

42. Goto Y, Tassel C, Noda Y, Hernandez O, Pickard CJ, Green MA, et al. Pressure-Stabilized Cubic Perovskite Oxyhydride BaScO2H. *Inorg Chem* (2017) 56:4840–5. doi:10.1021/acs.inorgchem.6b02834

43. Yamamoto T, Zeng D, Kawakami T, Arcisauskaite V, Yata K, Patino MA, et al. The Role of π-blocking Hydride Ligands in a Pressure-Induced Insulator-To-Metal Phase Transition in SrVO2H. *Nat Commun* (2017) 8. doi:10.1038/s41467-017-01301-0

44. Baeumer C, Li J, Lu Q, Liang AY-L, Jin L, Martins HP, et al. Tuning Electrochemically Driven Surface Transformation in Atomically Flat LaNiO3 Thin Films for Enhanced Water Electrolysis. *Nat Mater* (2021) 20:674–82. doi:10.1038/s41563-020-00877-1

45. Lee K, Goodge BH, Li D, Osada M, Wang BY, Cui Y, et al. Aspects of the Synthesis of Thin Film Superconducting Infinite-Layer Nickelates. *APL Mater* (2020) 8:041107. doi:10.1063/5.0005103

Publisher's Note: All claims expressed in this article are solely those of the authors and do not necessarily represent those of their affiliated organizations, or those of the publisher, the editors, and the reviewers. Any product that may be evaluated in this article, or claim that may be made by its manufacturer, is not guaranteed or endorsed by the publisher.